The effect of masonry infill walls on the reinforced concrete frames behavior under lateral load

Ismail Layadi, Ali Messabhia, Jean-Patrick Plassiard, Olivier Plé

Journal of Materials and Engineering Structures

Research Paper

The effect of masonry infill walls on the reinforced concrete frames behavior under lateral load

Ismail Layadi [a,b,], Ali Messabhia [a], Jean-Patrick Plassiard [b], Olivier Ple [b]*

[a] *Univ. Larbi Tebessi, Applied Civil Engineering Laboratory, 12002 Tebessa, Algeria*

[b] *Univ. Grenoble Alpes, Univ. Savoie Mont Blanc, UMR 5271 CNRS, LOCIE, 73000 Chambery, France*

ARTICLE INFO

Article history:

Received : 21 July 2019

Revised : 23 November 2019

Accepted : 2 December 2019

Keywords:

Infilled frames

Masonry

Digital Image Correlation technique

In-plane behavior

ABSTRACT

The reinforced concrete structures with masonry infill walls are widely used to construct buildings in Algeria, as in many parts of the world. According to earthquake analysis, this type of construction can undergo serious damage under seismic load. The interaction between the infill wall and the surrounding reinforced concrete structure is considered a key parameter, which could trigger damage and even collapse in self-stable frame buildings. To study the behavior of this type of structures and the wall–frame interaction, four half-scale single-storey, single-bay reinforced concrete unfilled and unfilled frames were constructed and tested under in-plane lateral load. Furthermore, the experimental results were analyzed using the Digital Image Correlation (DIC) technique giving a detailed analysis of displacement and strain fields. The wall–frame interaction was evaluated in terms of displacement field evolution and interface slip in the contact contour. The masonry infill wall demonstrated a significant influence on the in-plane lateral response of this type of structure. The analysis of the results of the experiment are discussed in this paper.

1 Introduction

In many parts of the world, including Algeria, reinforced concrete buildings with masonry infill walls are the most common building type. With regard to structural analysis and design, infill walls are often overlooked in design codes and considered as non-structural elements. Their contribution to lateral load resistance is ignored, leading to considerable inaccuracy in strength prediction. However, according to earthquake analysis, this type of structures can be severely damaged, essentially due to the strong interaction between the infill wall and its bare frame. This can lead to complex failure mechanisms and even collapse in self-stable frame buildings. Figure 1 shows the damage of this type. Previous researches have also confirmed this aspect through further experimental [1-4] and numerical studies [5-7], indicating that the presence of infill masonry walls can dramatically affect the response of this type of structure in terms of structural strength, stiffness

* *Corresponding author. Tel.: +33605721414.*
E-mail address: ismail.layadi@univ-smb.fr

e-ISSN: 2170-127X,

RESEARCH REVIEW of Sciences and Technologies

and energy dissipation capacity. Several parameters including geometric configurations, mechanical properties of infill and frame members, reinforcement details, relative stiffness and strength considerably influence and add to the complexity of this problem. Moreover, the quality of workmanship and local construction techniques affect the response of such structures [3]. In some cases, frames infilled with masonry showed up to three time greater stiffness than the unfilled frames, depending on the infill stiffness relative to the bare frame [8]. Moreover, the infilled frame, at a relatively low lateral load, acts as a monolithic system. However, the increase in loading leads to the separation of the infill wall from its bare frame, creating the equivalent diagonal strut mechanism (Figure 2a) [9]. Failure, in this case, could occur first in either the wall or the bare frame (Figure 2b). For more details about failure modes of infilled frames, one can refer to [3] and [10-11].

(a) (b)

Fig. 1 -Seismic damage in reinforced concrete infilled frames : Bingöl earthquake, Bingöl 2003 [12] (a) and Boumerdes earthquake, Boumerdes 2003 [13] (b)

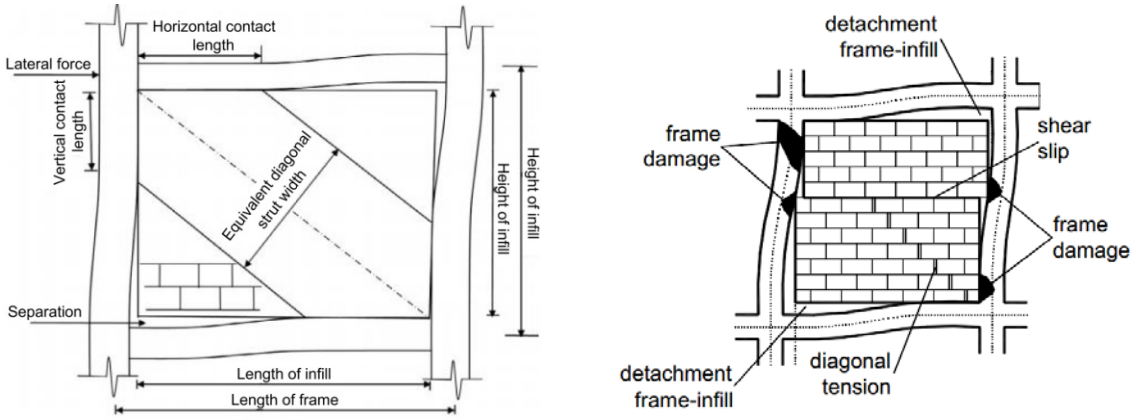

(a) (b)

Fig. 2- Behavior of masonry-infilled frame under lateral loading : diagonal strut mechanism [3] (a) and failure modes [11] (b)

Furthermore, most previous experimental studies on masonry infilled frames used a contact instrumentation measurement (linear variable differential transformer [LVDT] sensors and gauges) [8], [14], [4], for data acquisition and analysis, but such instrumentation does not provide a complete understanding of the frame–infill interaction, and only the overall behaviour, in this case, will be captured. Also, it can be altered by the cracks occurring during the test. Recently, a non-contact DIC technique appeared to be a powerful tool providing a detailed analysis of this type of structure [15-18]. The technique performs a detailed analysis throughout the test and can assess the displacement and strain fields of the specimen surface in the deformed state under loading. Its application to a reinforced concrete masonry infilled frame was first performed by [15]. In that work, the diagonal strut approach was experimentally evaluated. The diagonal compressive strut has been validated during the hardening phase of the loading providing also its angle of inclination. In the softening phase, a different failure

mechanism was observed; the diagonal inclined bands have changed to horizontal. However, neither the frame members failure mechanisms have been evaluated, nor the wall-frame interaction was provided.

Ghorbani et al [17] has also used DIC technique to visualize the loading-resistance mechanisms and failure modes in three confined masonry walls under in-plane lateral loading. Based on DIC results, it was observed that the development of the diagonal strut mechanism was clearly identified in the case of specimen with adequate reinforcement details especially at the beam-column connection. In the case of specimen with substandard details, the diagonal strut did not fully develop due to the beam-column connection opening (see [17] for more details). Nevertheless, no critical evaluation explains show the shear failure of the beam-column connection interacts with the diagonal strut action of the wall if any. Further, the same authors [17] evaluated the integrity of confined masonry walls by means of interface slip (discontinuity) between masonry infill and reinforced concrete tie column. The interface slip has been assessed using the displacement profile from DIC measurements. As a result, a negligible slip was reported indicating that the masonry infill acted monolithically with the reinforced concrete frame all along the test. Such behaviour is particularly exhibited in the case of confined masonry walls due to the full wall-frame contact consequent to the construction sequence of the wall, i.e., the construction of the wall before the reinforced concrete frame was cast, thus are fully integrated. In masonry walls unfilled after the construction of the reinforced concrete frame, the case of our study, the monolithic behaviour could be expected only at a relatively low lateral load [9]. The increase in loading can lead to the separation of the infill wall from its bare frame due to the initial lack of fit or gap between the infill wall and the surrounding frame.

To improve our understanding of the seismic performance of this type of structure, the DIC technique is used in our work to investigate the behaviour of four reinforced concrete infilled and unfilled frames tested under in-plane lateral loading. Specimens were constructed with a double masonry wall since this configuration fully reflects the current construction method in Algeria. The failure sequence and the wall-frame interaction has been evaluated by means of incremental strain maps, displacement fields evolution and interface slip in the contact contour from DIC measurements. The reason behind using an incremental analysis instead of the one regressive to the initial state used in the previous works is to have an insight into the behaviour evolution between each step of loading, i.e., what intervenes between the chosen steps and what disappears. Experimental results using the DIC technique are then presented and discussed.

2 Experimental program

2.1 Description of the specimens tested

Preparation, construction and experimental testing were carried out jointly between the LGCA Laboratory of Tebessa University and LOCIE Laboratory of Savoie Mont Blanc University. The experimental program consists of the test setup of four single-storey, single-bay reinforced concrete frames. Two of them were infilled with masonry bricks, whereas the other two remained unfilled. The aim was to define the various failure modes and behaviour of both infilled and unfilled frames under in-plane lateral loading and to verify the repeatability of the two loading cases: The monotonic and the loading/unloading cycles.

The geometry and reinforcement details of the specimens tested are shown in Figure 3. The dimensions of the specimens were chosen based on a 1:2 scale, with a height: length ratio of about 3:4, corresponding to a typical frame building constructed in Algeria (3 m high and 4 m long). In this case, the specimens tested were 152 cm high and 206 cm long. Columns and beams had a 25×25 cm square section, whereas a section measuring 30×40 cm was adopted for the base beam (Figure 3a-b).

The base beam, which is considered a rigid support to the infilled frame, ensured the continuity of reinforcement with the bare frame, as in a real configuration. Each set of specimens (two infilled and two unfilled) was cast at the same time. The specimen construction was governed by the typical Algerian design [19, 20] and seismic rules [21]. The infill was a double masonry wall constructed after curing the reinforced concrete frame with a 5 cm air gap, as shown in Figure 4.

The masonry elements used were locally manufactured, mainly hollow bricks in agreement with the NF P13-301 standard [22] measuring 10×20×30 cm (See Figure 4a), arranged in a running bond system with a 10 mm bed and head mortar joints. Steel bars measuring 12 and 6 mm were used in the specimen's construction for longitudinal and transverse reinforcement, respectively. The main mechanical properties of the materials used were evaluated and are summarized in Table 1.

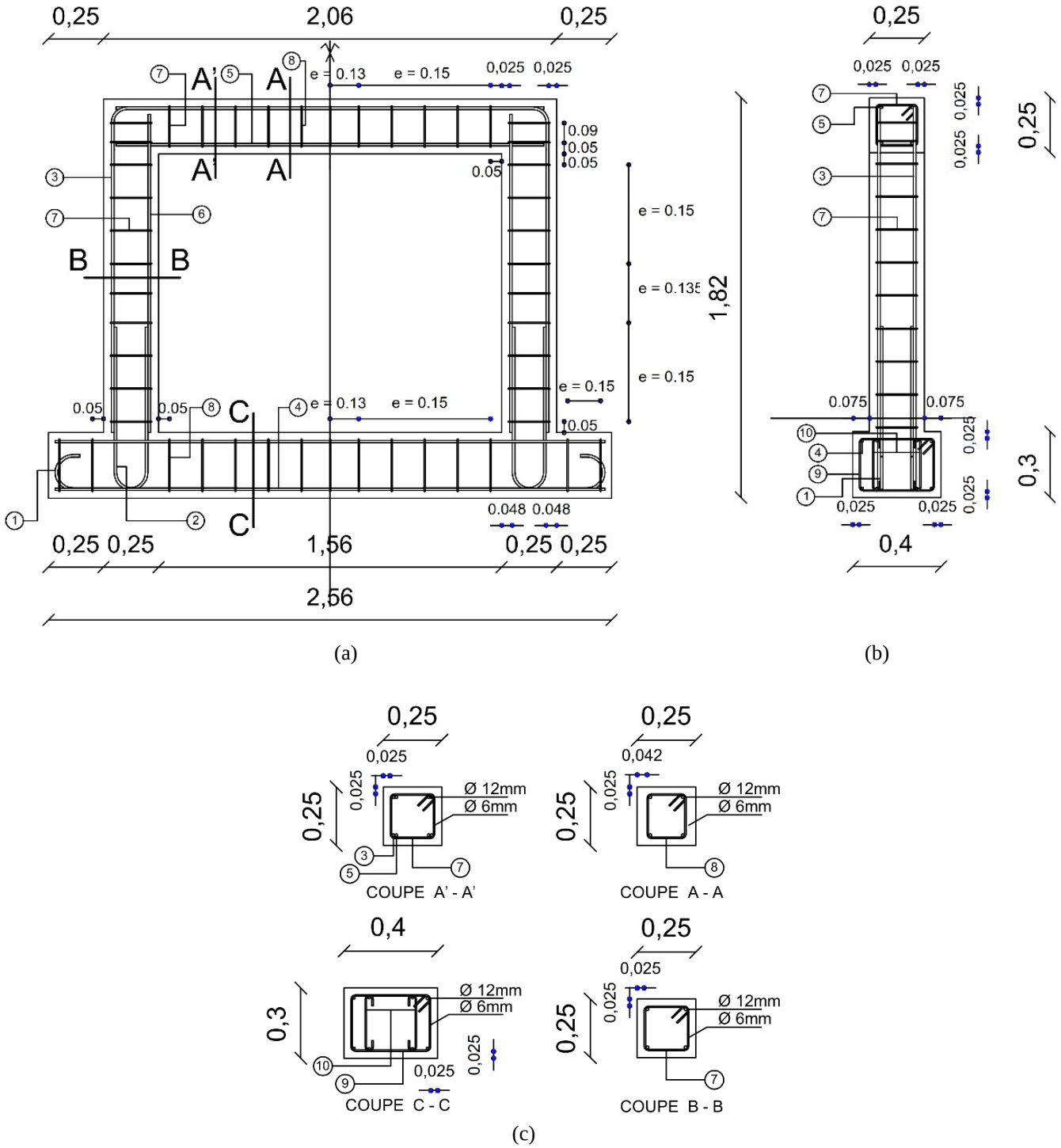

Fig. 3-Dimensions and reinforcement details of the specimens tested (dimensions in m) : front view (a), lateral view (b) and sections details (c)

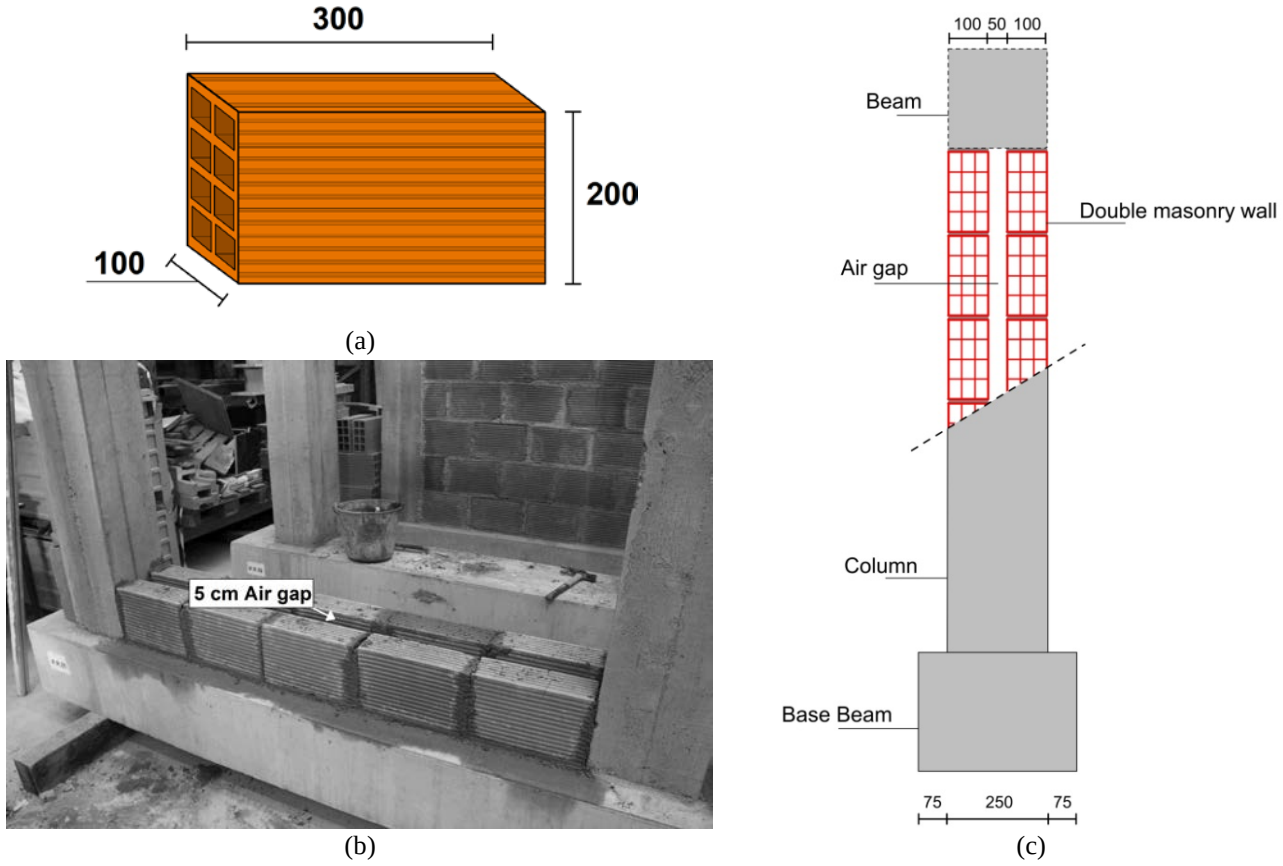

Fig. 4-Construction method for masonry double wall (dimensions in mm) : dimensions of the brick element (a), (b) and (c) double masonry wall details

Table 1 - Main mechanical properties of the materials used

Material	Main properties	Test standard	Average (MPa)
Concrete (bare frames)	Compressive strength	NF EN 12390-3 [23]	34.3
	Tensile strength	NF EN 12390-5 [24]	3.5
	Secant modulus[a]	NF EN 1992-1-1 [25]	15000
Concrete (infilled frames)	Compressive strength	NF EN 12390-3 [23]	27.5
	Tensile strength	NF EN 12390-5 [24]	2.9
	Secant modulus[a]	NF EN 1992-1-1 [25]	15700
Mortar	Compressive strength	NF EN 1015-11 [26]	14.9
	Flexure strength	NF EN 1015-11 [26]	3.9
Brick unit	Compressive strength (Orthogonal to holes)	-	0.8
	Compressive strength (Parallel to holes)	-	4.6
Masonry wallets	Normal compressive strength	NF EN 1052-1 [27]	0.73
	Diagonal shear strength	ASTM E 519-02 [28]	0.26
12ϕ Steel bar	Yield strength	-	501.2
6ϕ Steel bar	Yield strength	-	387.4

[a] Calculated as the slope of the line connecting the origin to 40 % of the peak strength according to the EN 1992-1-1 standard [25] and [29]

2.2 Test set-up and instrumentation

Test specimens were placed on a testing steel frame and were subjected to a combination of vertical and lateral in-plane loading by means of three actuators (See Figure 5b). In this respect, a constant vertical load was first applied by means of two electric actuators, VE1 and VE2, with a 120 kN capacity for each. The two actuators, representing the dead load of the upper floor acting on the beam, are a controlled force applied in 10 kN increments until reaching a vertical preload of 40 kN each, and it is kept constant throughout the rest of the test. The vertical load of the upper floors transmitted via the columns by axial forces is neglected due to the laboratory equipments limitation. In the second step, lateral horizontal displacement was applied on the beam's level with a 300 kN hydraulic actuator. This displacement was controlled by ± 1 mm increments until failure at a rate of 1 mm/min. The specimens are maintained on the testing steel frame by means of three boundary conditions: clamping jaws (CL1) are used to prevent out-of-plane tilting and to center the specimen with respect to the actuator. Then the vertical tie rods and steel shims prevent toppling and horizontal sliding behaviour (CL2 and CL3, respectively) (See Figure 5b). An UPN300 steel beam and a rolling cylinder system were placed on the frame's top, ensuring a vertical distribution of the preload, while the horizontal displacement was still free throughout the test (Figure 5a).

For data acquisition, the DIC technique was used to assess the displacement and strain fields of the specimen surface in the deformed state under loading. The DIC setup is presented in Figure 5c. A professional camera with a resolution of 16 Megapixels was placed facing the specimen with two light sources (projectors) to ensure permanent lighting on the wall surface. Because of the homogeneous nature of the wall, a painted speckle was added on the front surface to create the required contrast. For image processing and analysis, the 7D software developed by Vacher et al. [30] was used. All data acquisitions were then performed using a central acquisition unit and an acquisition system for recovering data results with regard to force and displacement of the three actuators, and the image recording.

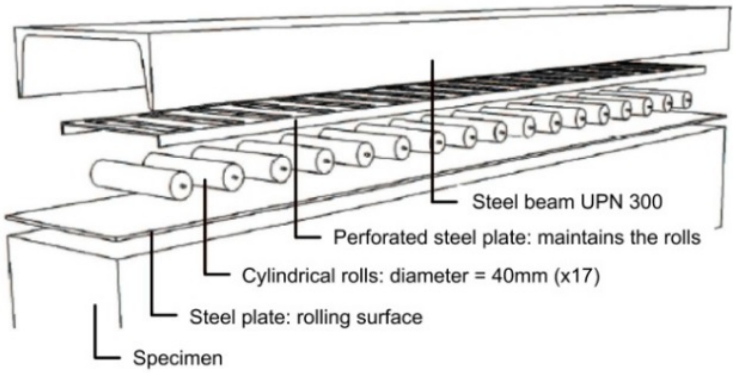

(a)

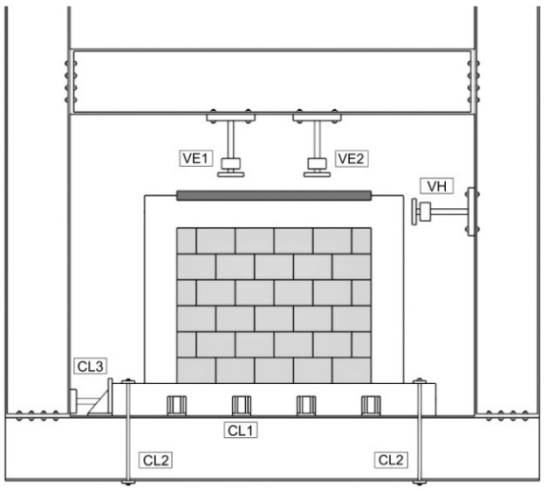

(b)

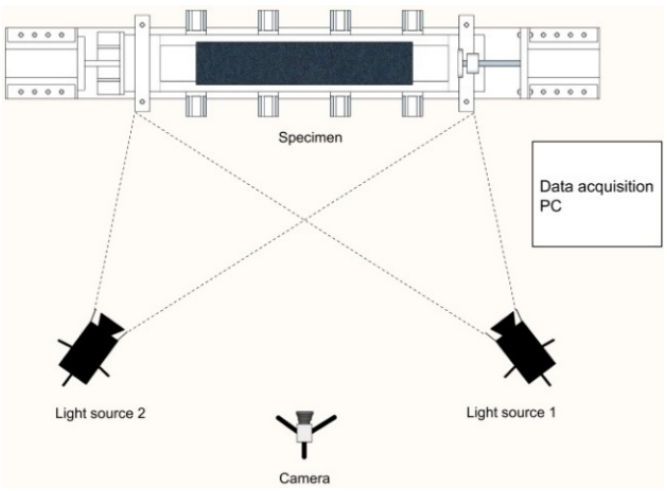

(c)

Fig. 5-Experimental test set-up : the rolling cylinder system (a), testing the steel frame (b), and the DIC experimental scheme (c)

3 Results and discussion

3.1 Behavior and failure modes using the DIC analysis

The response of the specimens tested is highlighted in Figures 6–9, with respect to the load-displacement relationship and the deformation pattern recorded using the DIC technique. The analysis was carried out in incremental, i.e., the image in the considered step is compared to that of the previous one (the image at point A is compared with the initial of point 0, the image of point B with that of point A, etc.). The values of the lateral load and the lateral displacement at debonding initiation, the first crack (in infill panel and frame members) and the peak level are summarized in Table 2.

Using an incremental strain map, the analysis of the results showed a similar deformation mechanism in both bare frames P.S.01 and P.S.02. At step point A (Figures 6-7), cracks were firstly developed in the left beam–column connection. A vertical flexural crack was also observed in the beam near the right beam-column connection for both specimens. Cracks in the right beam-column connection were then developed at step point B. A wider diffusion of cracks in the left side was also highlighted resulting in a more decreased stiffness up to the peak load of 76.1 kN (corresponding to 24.3 mm of lateral displacement) for P.S.01 and 76.4 kN (15.9 mm of lateral displacement) for P.S.02. A localized crack in the already damaged zones at the beam-column connections was then developed leading to the failure of the bare frames due to the flexural mechanism (step point C in Figures 6-7). Except the few flexural cracks that appeared at the bottom of the columns in the case of specimen P.S.02 (point B, Figure 7), no other cracks were observed in the columns of the two bare frames. In fact, both specimens exhibited significant ductility since post-peak resistance underwent a slight decrease, even for the displacements where the order of magnitude is two times larger than that measured at the peak resistance.

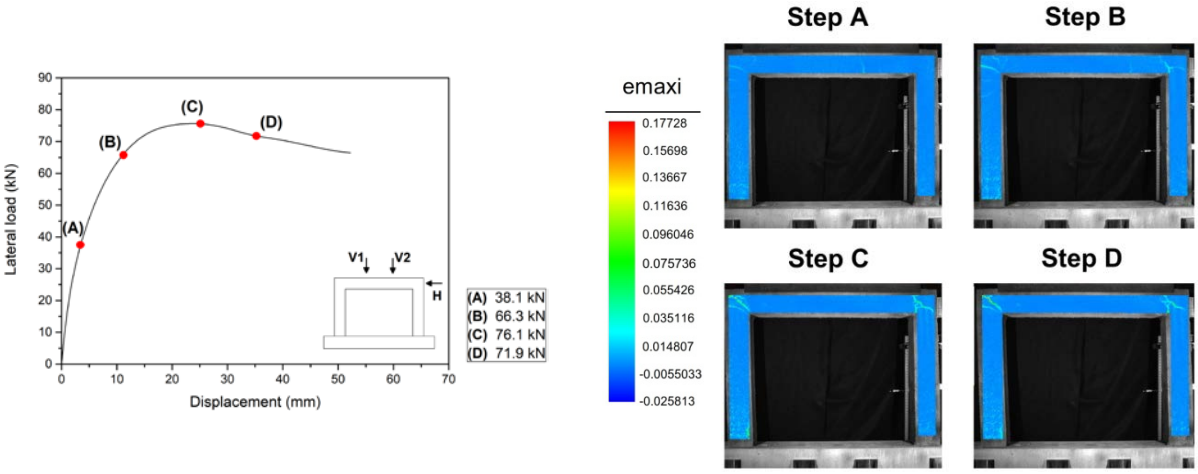

Fig. 6-The DIC strain fields for specimen P.S.01

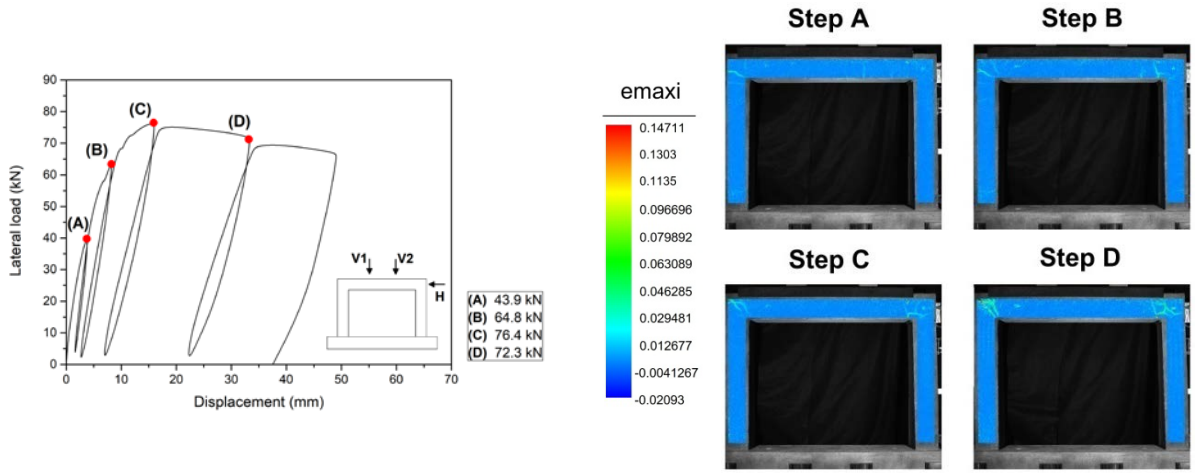

Fig. 7-The DIC strain fields for specimen P.S.02

Figure 8 shows the strain fields for specimen P.R.01. At low levels of lateral load, (step point A, 52.4 kN of lateral load corresponding to displacement of 0.59 mm), significant deformation starts to appear at the upper left contact area between the infill and the surrounding frame. This is related to the construction method used in this work. The deformation represents a debonding initiation between the infill and the frame members, since the infill wall was constructed after the bare frame, resulting in a non-negligible gap between the infill wall and the surrounding frame. These observations were also identified in the work of [15]. However, this result differs from the case of confined masonry for which the phenomenon was not reported [17]. When the debonding mechanism is fully developed at the contact contour, cracks start to develop in bed and head joints in the center and upper right corner of the panel (step point B in Figure 8). The first crack observed in the frame members was a shear crack in the right beam-column connection (step point C), after which diagonal stepped cracks started to develop from the center of the panel. The excessive shear force from the diagonal strut resisting mechanism exhibited by the infill wall explains the shear crack observed in the beam-column connection. From step point C to D, the diagonal stepped bed and head joints cracks changed to splitting cracks of brick units causing the decrease of stiffness observed in the force-displacement curve. The diagonal cracks became more pronounced and largely diffused at the peak load (step point E, 196.7 kN of lateral load and 12.2 mm of displacement) and extended progressively to the corners in a single dominant diagonal. Bed joint sliding also developed near the 1/3 height of the wall-right column contact. Therefore, the failure of the specimen coincided with the full development of the diagonal cracks together with the opening of the right beam-column connection. Flexural cracks at the mid-height of the right column were also observed. A large opening of the dominant diagonal crack characterized the specimen behavior at the post-peak level (step F).

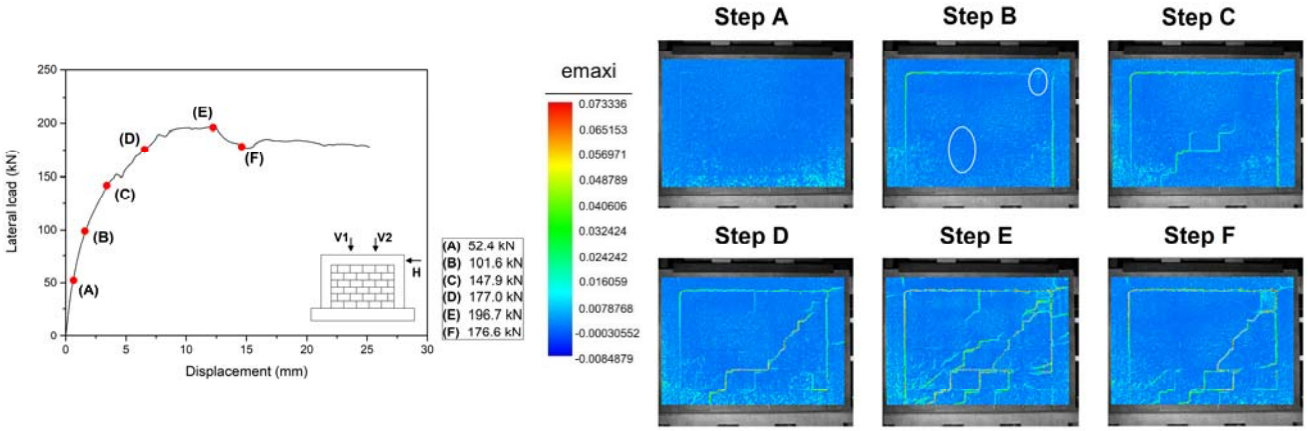

Fig. 8-The DIC strain fields for specimen P.R.01

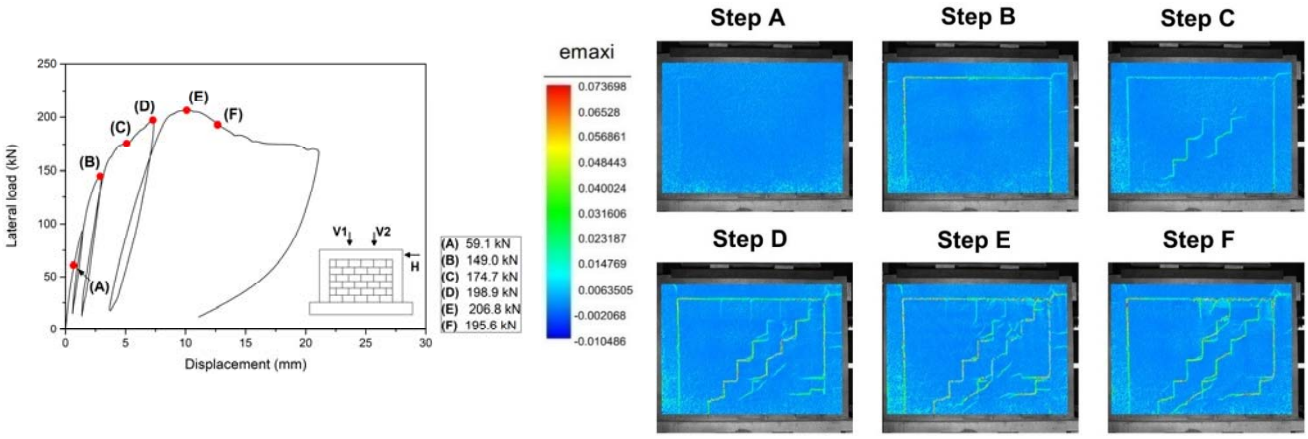

Fig. 9-The DIC strain fields for specimen P.R.02

Different schemes of cracks characterized the response of specimen P.R.02, but with a same failure mechanism, (Figure 9). The debonding mechanism was also developed at the entire contact contour (step point A, 59.1 kN of lateral load corresponding to displacement of 0.64 mm). However, unlike specimen P.R.01, cracks were firstly developed in the frame members (step point B). This can be explained by the local shear forces acting on the beam-column connection due to the diagonal strut resisting mechanism of the wall. Also, cracks in the infill wall were predominantly diagonal. They started from step point B to C and are characterized by two parallel diagonal staircase bed and head joints cracks. Few flexural cracks at the mid-height of the right column were also observed at step point D. Similar to specimen P.R.01, the failure was triggered by the full development of the diagonal cracks with the opening of the beam-column connection (step point E, 206.8 kN of lateral load and 10.1 mm of displacement). In post-peak level (point F, Figures8-9), a high concentration of deformations was observed at the upper right corner of the wall leading to the crushing of the brick elements in both specimens.

Table 2 - Summary of the specimens' primary results

Frame type	Loading type	Debonding initiation		First crack in infill panel		First crack in frame members		Peak level	
		F (kN)	d (mm)	F (kN)	d (mm)	F (kN)	d (mm)	F (kN)	d (mm)
Bare frame P.S.01	Monotonic	-	-	-	-	25.55	1.84	76.1	24.3
Bare frame P.S.02	Loading/unloading	-	-	-	-	30.11	2.16	76.4	15.9
Infilled P.R.01	Monotonic	52.4	0.59	101.6	1.65	123.8	2.61	196.7	12.2
Infilled P.R.02	Loading/unloading	59.1	0.64	161.7	3.77	141.0	2.53	206.8	10.1

3.2 Lateral strength and ductility

In terms of lateral load resistance, the specimens tested with the same frame type reached a very close maximum lateral load F_{max} independently from loading process (Figure10 and Table 3). P.S.01 and P.S.02 bare frames had a maximum lateral load of 76.1 kN and 76.4 kN, whereas a maximum of 196.7 kN and 206.8 kN were recorded for P.R.01 and P.R.02, respectively. Taking F_{max} ratio of bare frames equal to 1, this corresponds to almost three times greater lateral load resistance for infilled frames compared to bare frames, 2.6 and 2.7, respectively. Similar differences also reported in past studies [1], [31], [8] and [4]. This confirms the fact that masonry infill allows the structure to obtain a significant increase in the lateral strength.

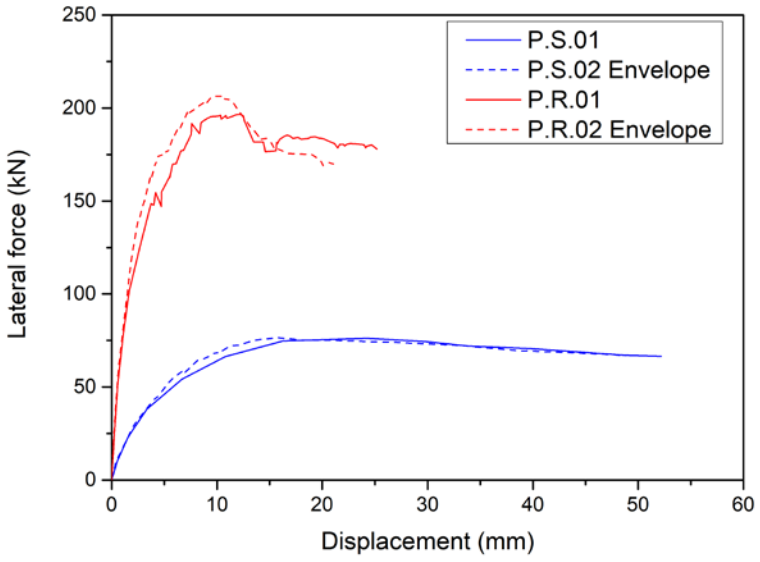

Fig. 10-The displacement ductility ratio for all specimens

Table 3 -The specimens' lateral strength and ductility results

Frame type	F_{max} (kN)	F_{max} ratio	δ_1 (mm)	δ_{max} (mm)	δ_2 (mm)	μ
Bare frame P.S.01	76.1	1	10.8	24.3	52.2	4.8
Bare frame P.S.02	76.4	1	8.8	15.9	49.0	5.6
Infilled P.R.01	196.7	2.6	5.8	12.2	25.2	4.3
Infilled P.R.02	206.8	2.7	4.7	10.1	19.0	4.0

The plastic deformation capacity of the tested specimens is also evaluated by means of the displacement ductility factor μ. This factor is calculated as the ratio of the ultimate displacement δ_2 to yield displacement δ_1 as defined in [32]. The yield and ultimate displacements correspond to the lateral displacement at 85% of maximum lateral load from the load-displacement curve in the ascending and descending parts, respectively (Figure11a). In the case of specimen P.R.01, the lateral displacement at the ultimate load is taken as the last displacement obtained at the end of the test due to failing to attain 85% of the lateral load (which corresponds to almost 90 % of peak load). As indicated in Figure11b and Table 3, bare frames P.S.01 and P.S.02 exhibited a more ductile behaviour, about 11.6% and 40% compared to infilled frames P.R.01 and P.R.02, respectively. Ductility factor of 4.8 and 5.6 were obtained for P.S.01 and P.S.02 compared to 4.3 and 4.0 for P.R.01 and P.R.02, respectively. Similar results have been reported by Jiang et al [33] and Essa et al [31]. Even though specimen P.S.01 failed at a relatively larger displacement level ($\delta_{max} = 24.3\ mm$), specimen P.S.02 showed greater ductility, about 16.7 % than P.S.01. In the case of infilled frames, the difference in ductility between P.R.01 and P.R.02 is less significant, about 7.5%.

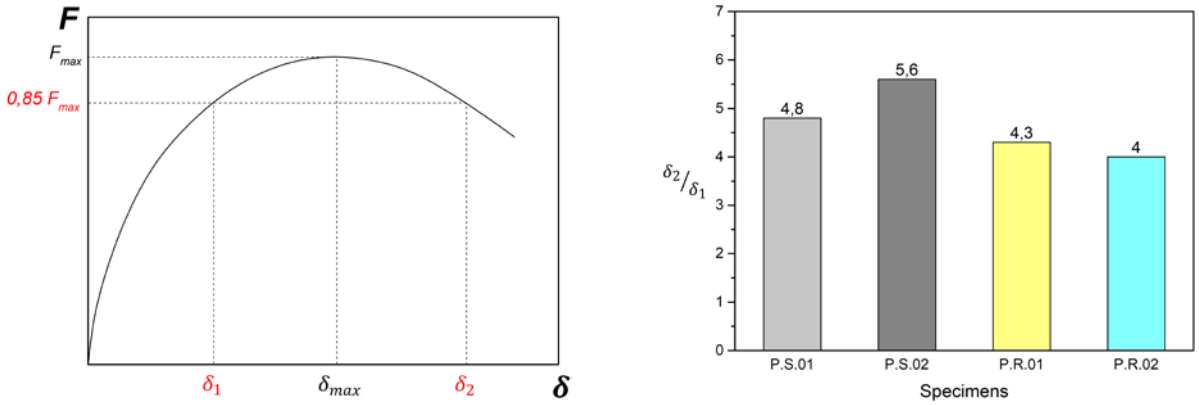

(a) (b)

Fig. 11-Ductility evaluation for all specimens : definition of ductility parameters (a) and displacement ductility ratio (b)

3.3 Lateral stiffness

As indicated in Table 4, the initial lateral stiffness K_0 of infilled frames P.R.01 and P.R.02 was 5.3 and 4.4 times that of bare frames P.S.01 and P.S.02. Related results were found in the literature [34], [35]. The secant stiffness K_s of the loading/unloading cycles in specimens P.S.02 and P.R.02 was also calculated considering the slope of the line connecting the extreme points of each cycle. Results are summarized in Table 5. Figure 12 shows the stiffness degradation ratio with respect to the lateral displacement ratio. The stiffness ratio is calculated as the ratio of the secant stiffness for each cycle to the initial stiffness, while the displacement ratio is calculated as the ratio of displacement for each cycle to the displacement at peak level. Significant information can be deduced. First, significant stiffness degradation was observed through the loading/unloading cycles of both specimens (Figure 12). Also, a comparable stiffness loss was found between the two specimens from the beginning of the test up to the peak load level, about 67.1 % and 57.1 % for P.S.02 and P.R.02, respectively. However, P.R.02 underwent a considerable loss in stiffness in post-peak level from 47.6 kN/mm (third cycle) to 15.3 kN/mm (fourth cycle) at about 67.8 % compared to 31.3 % for P.S.02 (from 8.3 kN/mm to 5.7 kN/mm). The excessive damage of the masonry infill wall in the case of P.R.02 was the reason behind losing more stiffness progressively, especially after peak loading (See Figure 12 and Table 5).

Table 4 -The Specimens' initial lateral stiffness results

Reference	Initial stiffness K_0 (kN/mm)	Initial stiffness ratio
P.S.01	19.0	1
P.S.02	25.2	1
P.R.01	101.1	5.3
P.R.02	110.9	4.4

Table 5 - Stiffness degradation in loading/unloading cycles

Reference	K_0(kN/mm)	Stiffness per cycle K_s (kN/mm)				
		First	Second	Third	Fourth	Fifth
P.S.02	25.2	16.1	11.3	8.3	6.4	5.7
P.R.02	110.9	97.8	81.4	47.6	15.3	-

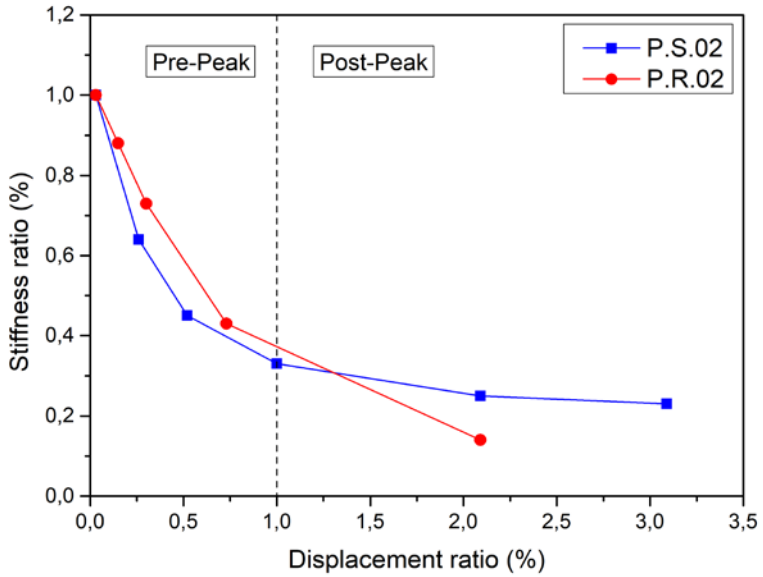

Fig. 12-Stiffness degradation in the loading/unloading cycles

3.4 Energy dissipation capacity

The energy dissipation of the specimens tested under the loading/unloading cycles is also calculated and presented in Figure 13 and Table 6. To have a better comparison of the results, only the cycles carried out up to the peak load are considered. The energy dissipated for each cycle was calculated as the area enclosed by the hysteresis loops in the load-displacement curve. The summation of the energy dissipated in each cycle gives the accumulated energy dissipation, also presented in Table 6.Figure 13a shows the evolution of the accumulated energy dissipation of P.S.02 and P.R.02 with respect to the lateral displacement ratio calculated as the ratio of the displacement for each cycle to the displacement at peak level. For both specimens, the energy dissipated is proportional to the lateral displacement. For more clarity, the analysis was carried out with respect to the cycles as shown in Figure 13b. The bare frame P.S.02 slightly dissipated more energy compared to the infilled frame P.R.02, about 6.7 %. This differs from the results found in the literature where the masonry infill wall allowed the structure to dissipate more energy ranging from a ratio of 1.3 to 3.3 times [2], [31], [33] and [4]. In fact, the pushover loading performed in this work (loading/unloading cycles) differs from that of the literature, generally performed with a cyclic loading (with positive and negative parts). This aspect can influence the results in terms of the energy dissipated.

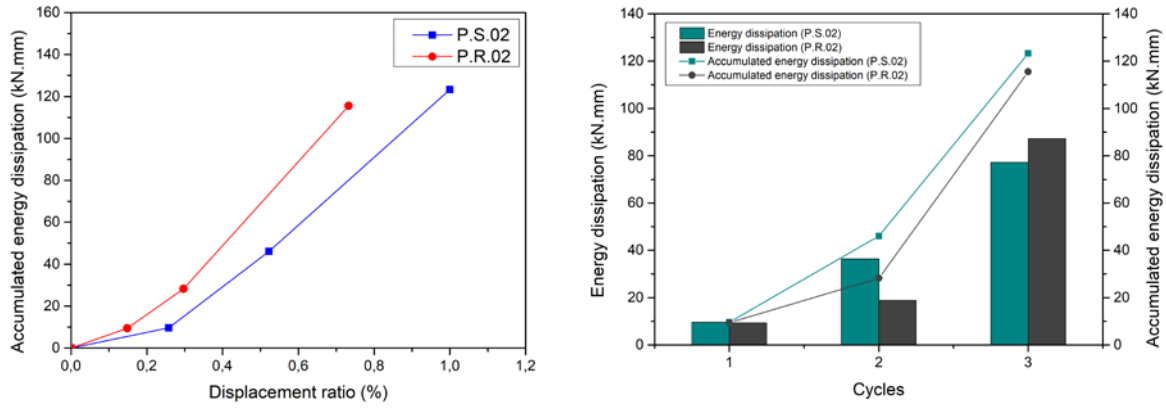

(a) (b)

Fig. 13- Energy dissipation capacity of specimens P.S.02 and P.R.02 : accumulated energy dissipation as a function of displacement ratio (a) and energy dissipation as a function of cycles

Table 6 - Energy dissipation in the loading/unloading cycles

Reference	Energy dissipated per loading/unloading cycle (kN.mm)			Total accumulated energy dissipation (kN.mm)
	First	Second	Third	
P.S.02	9.6	36.4	77.3	123.3
P.R.02	9.4	18.8	87.3	115.5

3.5 Wall-frame interaction

The Wall–frame interaction during the test was investigated using the DIC technique in terms of principal directions of deformation, interface slip between the infill wall and the surrounding reinforced concrete frame and displacement field evolution. First, the principal directions of deformation were evaluated at the debonding and peak level (corresponding to step point B and E in Figure 9, respectively) and presented in Figure14. At the debonding level (Figure14a), the principal directions of deformation indicated a shear development through almost the entire wall-frame contact contour. Tensile and compression stresses were also noticed in the upper left and right corner, respectively. The phenomenon continues until the diagonal failure of the wall. At the peak load (Figure14b), the opening of the diagonal cracks is clearly visible with a less significant shear observed at the lower right level at about 1/3 of the wall height. This implies that, with increasing lateral load, masonry infill wall acts monolithically with the frame only in the lower part unlike most of the contour (same observations for the lower part in the left side). Similar results were reported for specimen P.R.01.

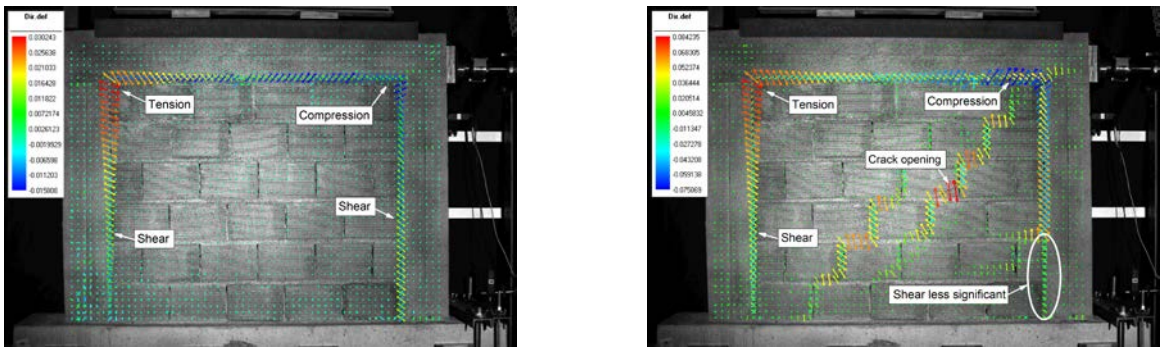

(a) (b)

Fig. 14 -Principal directions of deformations evaluation for specimen P.R.02 : at debonding (a) and peak levels (b)

To have an insight on the wall-frame integrity, the vertical displacement of two points on the same height, one on the masonry wall side (d_{yM}) and the other on the frame side (d_{yF}) for three levels (top, mid-height and bottom of the masonry wall), were identified and plotted (Figure 15).

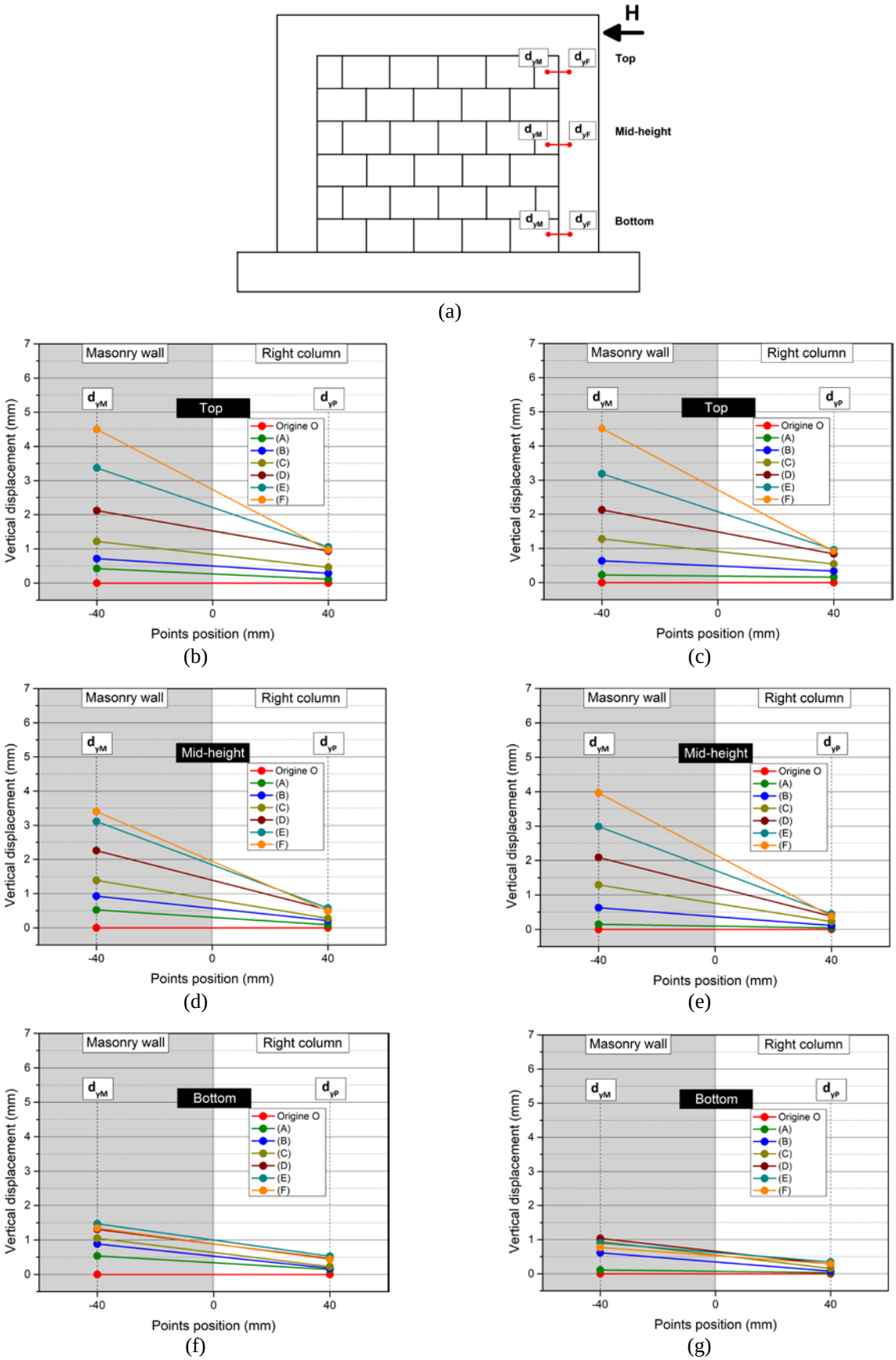

Fig. 15 -Interface slip computation at the wall-frame right contact : definition of the points identified (a), identification for specimen P.R.01 (b), (d) and (f), and for specimen P.R.02 (c), (e) and (g) corresponding to the top, mid-height and bottom level, respectively

The initial distance between the two adjacent points is 8 cm. As a first observation, a significant interface slip at the wall-frame contact is noticed for both specimens. It is worth noting that most of these relative displacements are generated before the peak strength. It seems that the monolithic behavior is no more representative of the interaction between the masonry and the frame, even for loading lesser than the peak strength. Furthermore, the vertical displacement in the infill wall (d_{yM}), compared to that of the frame side (d_{yF}), is much greater for the mid-height and top points, while the displacements are in the same range for the bottom point (Figure 15). This implies the existence of a sliding mechanism at the wall-frame interface of the contour. It can be noticed that the relative displacements are already present in the linear part of the behaviour (point A, Figures 8-9). The slip became significant from step point C, about 75% and 85% of the maximum lateral load, corresponding to 147.9 kN and 174.7 kN of lateral load, 4 mm and 5 mm of lateral displacement for P.R.01 and P.R.02, respectively (Figures 8-9). This can be explained by the aforementioned debonding mechanism in the contact contour. Due to the construction method used (i.e., building the wall after the reinforced concrete frame was cast), the existing initial gap at the contour allowed the sliding between the wall and the surrounding frame and their debonding.

The phenomenon is specific to the masonry infilled frames. In the case of confined masonry, where the wall is built before the frame, the behaviour is different. Based on the work of [17] in which frames with confined masonry were studied, the slip at the wall-frame interface is negligible. Therefore, it can be deduced that the contour in infilled masonry frames corresponds to a weakness that alter the lateral resistance mechanism, and do not allow reaching a lateral strength comparable to the one noticed for confined masonry [36].

Other information can be explored using the horizontal displacement fields shown in Figure 16. The displacement field was evaluated this time in the pre-peak, peak and post-peak levels (points C, E and F in Figure 9, respectively) for all three levels (top, mid-height and bottom). At the top and mid-height levels, the horizontal displacement has gradually increased as the lateral load increased, while the bottom level still had no significant displacement. Consequently, one can clearly notice the division of the displacement field of the infilled frame into upper and lower parts. The upper part tends to move separately from the lower part depending on the beam displacement after diagonal cracking of the masonry wall. This also confirms the observations drawn from principal directions of deformation and vertical displacement (Figures 14-15) and explains the lesser amount of slip observed at the bottom level for both the frame and infill sides. The higher displacement values observed at the beam level were due to sliding at the horizontal wall-beam interface explained by the inefficient filling of the gap between the wall and the reinforced concrete beam. Furthermore, it seems that the part of the right column located below the separation line is still transferring a part of the loading to the lower part of the masonry via a shear force. With the increase of the loading, this shear force increases the tension in the lower part of the masonry, creating a bed joint crack near the 1/3 height of the right column. This evolution of the masonry part following the displacement of the concrete frame made it difficult to establish an analytical prediction of the lateral stiffness and lateral strength of such structures with Strut-and-Tie methods [36].

Finally, the results obtained regarding the wall-frame interaction are consistent with those found in the literature. The masonry infill wall acts monolithically with its frame in the early levels of the test, and begins a significant debonding between the wall and the frame from a very high load. This moment is followed by the development of diagonal cracking. Most of the contour has undergone either significant slip or debonding. Nevertheless, the wall-frame debonding was not observed at all the contour and the monolithic behaviour became therefore restricted at the bottom right and left sides of the wall. The two lower parts have not undergone a significant separation due to the opening of the diagonal cracks.

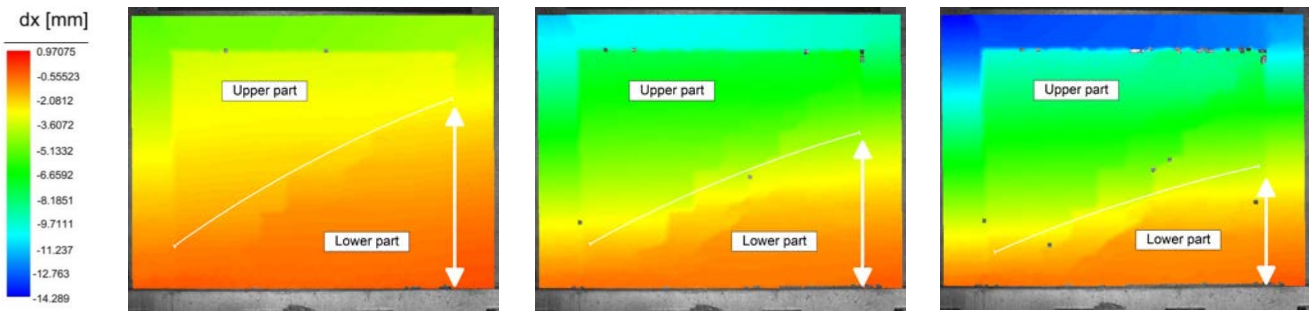

(a) (b) (c)

Fig. 16 -Horizontal displacement field for specimen P.R.02 at the pre-peak (a), peak (b) and post-peak level (c)

4 Conclusion

In this study, the masonry infill wall effect on the in-plane response of a reinforced concrete structure was experimentally investigated. An important finding was reported describing the actual performance of the wall–frame interaction throughout the test proving the effectiveness of the DIC technique. The main conclusions that can be drawn from the test results are:

- There is a good reproducibility of the results for the specimens tested with the same frame type regardless of the type of loading. Also, the incremental DIC analysis allowed a complete visualization of the failure scheme. Thus, the identified failure modes are consistent with those of the literature.
- A localized crack opening in the beam-column connection triggered the failure of both bare frames due to flexural mechanism. In the case of infilled frames, the classic diagonal crack mechanism was verified, extended to corners in a single and double dominant diagonal.
- From the infilled frames cracks scheme, no causal link was observed between crack propagation in the infill wall and beam-column connections. For specimen P.R.01, cracks were firstly developed in the infill wall whereas cracks were developed first in the frame members in the case of specimen P.R.02 due to the diagonal strut resisting mechanism. However, the same failure mechanism was reported for the two specimens.
- The presence of the masonry infill wall improved the lateral load resistance of the structure, nearly three times higher than unfilled frames, but at the same time limited its ability to deform inelastically.
- Although the infilled frames showed greater lateral stiffness compared to the unfilled frames, the excessive damage of the masonry infill wall resulted in substantial stiffness degradation in the loading/unloading cycles. On the other hand, the loading/unloading type performed in this work did not provide a good overview on the energy dissipation capacity of the specimens. The dissipated energy obtained is therefore relatively close between P.S.02 and P.R.02, which differs from the usual cases in the literature, where it is admitted that infilled frames dissipate more energy than bare frames.
- The local construction sequence used proved to have a remarkable influence on the wall–frame interaction. Unlike confined masonry structures, the gap remaining between the infill wall and the surrounding frame resulted in adebonding effect at the wall–frame contact contour, which is the primer of an irreversible phenomenon. The monolithic behavior between the infill wall and the surrounding frame was then interrupted and became restricted to 1/3 of the wall-frame contact. Shear, tension and compression stresses characterized the wall-frame interaction consequently. A noteworthy slip between the infill wall and the corresponding bare frame was reported in this case.
- Finally, the DIC technique proved to be a powerful tool both qualitatively and quantitatively, allowing a more detailed analysis of the wall-frame interaction throughout the test.

Acknowledgements

The authors would like to express their gratitude to the financial support provided by the Ministry of higher education and scientific research of Algeria, LGCA laboratory of Tebessa University-Algeria and LOCIE laboratory of Savoie Mont Blanc University-France.

REFERENCES

[1]- A.B. Mehrabi, P.B. Shing, M.P. Shuller, J.L. Noland, Experimental evaluation of masonry-infilled RC frames. J. Struct. Eng-ASCE. 122(3) (1996) 228-237. doi:10.1061/(ASCE)0733-9445(1996)122:3(228)

[2]- J. Zovkic, V. Sigmund, I. Guljas, Cyclic testing of a single bay reinforced concrete frames with various types of masonry infill. Earthq. Eng. Struct. Dynam. 42(8) (2013) 1131-1149. doi:10.1002/eqe.2263

[3]- P. Haldar, Y. Singh, D.K. Paul, Identification of seismic failure modes of URM infilled RC frame buildings. Eng. Fail. Anal. 33(2013) 97-118. doi:10.1016/j.engfailanal.2013.04.017

[4]- S.H. Basha, H.B. Kaushik, Behavior and failure mechanisms of masonry-infilled RC frames (in low-rise buildings) subject to lateral loading. Eng. Struct. 111(C) (2016) 233-245. doi:10.1016/j.engstruct.2015.12.034

[5]- I. Koutromanos, A. Stavridis, P.B Shing, K. Willam, Numerical modeling of masonry-infilled RC frames subjected to seismic loads. Comput. Struct. 89(11-12) (2011) 1026-1037. doi:10.1016/j.compstruc.2011.01.006

[6]- P.G. Asteris, I.P. Giannopoulos, C.Z. Chrysostomou, Modeling of infilled frames with opening. Open Constr. Build. Technol. J. 6(1) (2012) 81-91. doi:10.2174/1874836801206010081

[7]- G.C. Manos, V.J. Soulis, J. Thauampteh, The behaviour of masonry assemblages and masonry-infilled R/C frames subjected to combined vertical and cyclic horizontal seismic-type loading. Adv. Eng. Softw. 45(1) (2012) 213-231.

doi:10.1016/j.advengsoft.2011.10.017
[8]- V. Sigmund, D. Penava, Influence of opening, with and without confinement, on cyclic response of infilled R-C frames–An experimental study. J. Earthq. Eng. 18(1) (2014) 113-146. doi:10.1080/13632469.2013.817362
[9]- P.B. Shing, A.B. Mehrabi, Behavior and analysis of masonry-infilled frames. Prog. Struct. Eng. Mater. 4(3) (2002) 320-331. doi:10.1002/pse.122
[10]- W.W. El-Dakhakhni, M. Elgaaly, A.A. Hamid, Three-strut model for concrete masonry-infilled steel frames. J Struct Eng. 129(2) (2003) 177-185. doi:10.1061/(ASCE)0733-9445(2003)129:2(177)
[11]- P.G. Asteris, S.T. Antoniou, D.S. Sophianopoulos, C.Z. Chrysostomou, Mathematical macromodeling of infilled frames: state of the art. J. Struct. Eng. 137(12) (2011) 1508–1517. doi:10.1061/(ASCE)ST.1943-541X.0000384
[12]- G. Özcebe, J. Ramirez, S.T. Wasti, A. Yakut, 1 May 2003 Bingöl Earthquake Engineering Report. Technical Report, Tubitak, NSF. 2003.
[13]- V. Davidovici, Boumerdes Earthquake of 21 May 2003, Preliminary Report, Algeria, 2003.
[14]- H. Okail, A. Abdelrahman, A. Abdelkhalik, M. Metwaly, Experimental and analytical investigation of the lateral load response of confined masonry walls. HBRC J. 12(1) (2016) 33-46. doi:10.1016/j.hbrcj.2014.09.004
[15]- N. Guerrero, M. Martinez, R. Picon, M.E. Marante, F. Hild, S. Roux, J. Florez-Lopez, Experimental analysis of masonry infilled frames using digital image correlation. Mater. Struct. 47(5) (2014) 873-884.
[16]- M. Eymard, Analysis of the mechanical behavior of the interface between an innovative thermal insulation coating and its structural support. PhD thesis, University of Grenoble, 2014.
[17]- R. Ghorbani, F. Matta, M.A. Sutton, Full-field deformation measurement and crack mapping on confined masonry walls using digital image correlation. Exp. Mech. 55(1) (2015) 227-243. doi:10.1007/s11340-014-9906-y
[18]- A. Furtado, H. Rodrigues, A. Arêde, H. Varum, Experimental evaluation of out-of-plane capacity of masonry infill walls. Eng. Struct. 111(C) (2016) 48-63. doi:10.1016/j.engstruct.2015.12.013
[19]- DTR C2-45, Masonry design and calculation rules, Technical document, CNERIB, Algiers, 1997.
[20]- DTR E2-4, Masonry works of small elements, Technical document, CNERIB, Algiers, 1997.
[21]- RPA99, Algerian seismic code RPA99/version 2003, Technical document, CGS, Algiers, 2003.
[22]- NF P13-301, Hollow clay bricks, French Standard for hollow bricks, 1974.
[23]- BS EN 12390-3, Testing hardened concrete - Part 3: Compressive strength of test specimens, British Standards Institution (BSI), 2019.
[24]- NF EN 12390-5, Testing hardened concrete - Part 5: Flexural strength of test specimens. AFNOR, 2019.
[25]- NF EN 1992-1-1, Eurocode 2: Design of concrete structures - Part1-1: General rules and rules for buildings, European Committee for Standardization, 2004.
[26]- BSI EN 1015-11, Methods of test for mortar for masonry - Part 11: Determination of flexural and compressive strength of hardened mortar. British Standards Institution (BSI), 1999.
[27]- BSI EN 1052-1, Method of test for masonry - Part 1: Determination of compressive strength. British Standards Institution (BSI), 1999.
[28]- ASTM E519-02, Standard Test Method for Diagonal Tension (Shear) in Masonry Assemblages, ASTM International, West Conshohocken, PA, 2002. doi:10.1520/E0519-02
[29]- C.C. Vu, Statistical size effects on compressive strength of concrete, PhD thesis, University of Grenoble, 2014.
[30]- P. Vacher, S. Dumoulin, F. Morestin, S. Mguil-Touchal, Bidimensional strain measurement using digital images. P. I. Mech. Eng. C-J. Mech. 213(8) (1999) 811-817. doi:10.1243/0954406991522428
[31]- A.S.A.T. Essa, M.R.K. Badr, A.H. El-Zanaty, Effect of infill wall on the ductility and behavior of high strength reinforced concrete frames. HBRC J. 10(3) (2014) 258-264. doi:10.1016/j.hbrcj.2013.12.005
[32]- F.J. Crisafulli, Seismic Behaviour of Reinforced Concrete Structures with Masonry Infills. PhD thesis, University of Canterbury, 1997.
[33]- H. Jiang, X. Liu, J. Mao, Full-scale experimental study on masonry infilled RC moment-resisting frames under cyclic loads. Eng. Struct. 91(2015) 70-84. doi:10.1016/j.engstruct.2015.02.008
[34]- C.V.R. Murty, S.K. Jain, Beneficial influence of masonry infills on seismicperformance of RC frame buildings. In: Proceedings of the 12th World Conference on Earthquake Engineering, Auckland, 2000, Paper No. 1790.
[35]- K.C. Stylianidis, Experimental investigation of masonry infilled RC frames. Open Constr. Build. Technol. J. 6(1) (2012)194–212. doi:10.2174/1874836801206010194
[36]- C. Belghiat, A. Messabhia, J.P. Plassiard, M. Guenfoud, O. Plé, P. Perrotin, Experimental study of double-panel confined masonry walls under lateral loading. J Build. Eng. 20(2018) 531–543. doi:10.1016/j.jobe.2018.09.001.